Cardiomyocyte-Specific STIM1 (Stromal Interaction Molecule 1) Depletion in the Adult Heart Promotes the Development of Arrhythmogenic Discordant Alternans

Marine Cacheux, Benjamin Strauss, Nour Raad, Zeki Ilkan, Jun Hu, Ludovic Benard, Stefan Feske, Jean-Sebastien Hulot, Fadi G Akar

Circulation: Arrhythmia and Electrophysiology

ORIGINAL ARTICLE

Cardiomyocyte-Specific STIM1 (Stromal Interaction Molecule 1) Depletion in the Adult Heart Promotes the Development of Arrhythmogenic Discordant Alternans

Marine Cacheux, PhD
Benjamin Strauss, PhD
Nour Raad, MD
Zeki Ilkan, PhD
Jun Hu, PhD
Ludovic Benard, PhD
Stefan Feske, MD
Jean-Sebastien Hulot, MD, PhD
Fadi G. Akar, PhD

BACKGROUND: STIM1 (stromal interaction molecule 1) is a calcium (Ca^{2+}) sensor that regulates cardiac hypertrophy by triggering store-operated Ca^{2+} entry. Because STIM1 binding to phospholamban increases sarcoplasmic reticulum Ca^{2+} load independent of store-operated Ca^{2+} entry, we hypothesized that it controls electrophysiological function and arrhythmias in the adult heart.

METHODS: Inducible myocyte-restricted STIM1-KD (STIM1 knockdown) was achieved in adult mice using an αMHC (α-myosin heavy chain)-MerCreMer system. Mechanical and electrophysiological properties were examined using echocardiography in vivo and optical action potential (AP) mapping ex vivo in tamoxifen-induced $STIM1^{flox/flox}$-$Cre^{tg/-}$ (STIM1-KD) and littermate controls for $STIM1^{flox/flox}$ (referred to as STIM1-Ctl) and for $Cre^{tg/-}$ without STIM deletion (referred to as Cre-Ctl).

RESULTS: STIM1-KD mice (N=23) exhibited poor survival compared with STIM1-Ctl (N=22) and Cre-Ctl (N=11) with >50% mortality after only 8-days of cardiomyocyte-restricted STIM1-KD. STIM1-KD but not STIM1-Ctl or Cre-Ctl hearts exhibited a proclivity for arrhythmic behavior, ranging from frequent ectopy to pacing-induced ventricular tachycardia/ventricular fibrillation (VT/VF). Examination of the electrophysiological substrate revealed decreased conduction velocity and increased AP duration (APD) heterogeneity in STIM1-KD. These features, however, were comparable in VT/VF(+) and VT/VF(–) hearts. We also uncovered a marked increase in the magnitude of APD alternans during rapid pacing, and the emergence of a spatially discordant alternans profile in STIM1-KD hearts. Unlike conduction velocity slowing and APD heterogeneity, the magnitude of APD alternans was greater (by 80%, $P<0.05$) in VT/VF(+) versus VT/VF(–) STIM1-KD hearts. Detailed phase mapping during the initial beats of VT/VF identified one or more rotors that were localized along the nodal line separating out-of-phase alternans regions.

CONCLUSIONS: In an adult murine model with inducible and myocyte-specific STIM1 depletion, we demonstrate for the first time the regulation of spatially discordant alternans by STIM1. Early mortality in STIM1-KD mice is likely related to enhanced susceptibility to VT/VF secondary to discordant APD alternans.

VISUAL OVERVIEW: A visual overview is available for this article.

Key Words: arrhythmias ■ calcium ■ discordant alternans ■ stromal interaction molecule 1 ■ ventricular fibrillation

https://www.ahajournals.org/journal/circep

WHAT IS KNOWN?

- STIM1 (stromal interaction molecule 1) is a calcium sensor originally known for its role in mediating calcium entry in response to endoplasmic reticulum calcium depletion in nonexcitable cells.
- In the heart, STIM1 regulates pathological hypertrophy by triggering store-operated calcium entry.
- Recent in vitro studies have suggested store-operated calcium entry-independent roles of STIM1 in the cardiomyocyte, namely modulation of SR calcium load.

WHAT THE STUDY ADDS?

- The present study explores the homeostatic role of cardiomyocyte STIM1 expression in the adult heart.
- Inducible cardiomyocyte-specific STIM1 depletion in adult mice caused accelerated mortality, in vivo, and a proclivity for arrhythmic behavior, ranging from frequent ectopy to pacing-induced ventricular tachycardia/fibrillation, ex vivo.
- Examination of the electrophysiological substrate revealed a spatially discordant alternans profile that likely gave rise to malignant ventricular arrhythmias.

STIM1 (stromal interaction molecule 1) is a single-pass transmembrane protein that acts as a luminal calcium (Ca^{2+}) sensor of the endoplasmic reticulum (ER).[1] In response to ER Ca^{2+} store depletion, STIM1 triggers store operated-calcium entry (SOCE) by interacting with plasma membrane channels, namely Orai1, to mediate the influx of Ca^{2+} from the extracellular space. Although initially identified and characterized in nonexcitable cells, STIM1-dependent SOCE has more recently been demonstrated in skeletal[2,3] and smooth muscle cells,[4] as well as fibroblasts[5,6] and cardiomyocytes.[7,8]

The expression of STIM1 is robust in the neonatal heart, where it plays a central role in the regulation of Ca^{2+} homeostasis and signaling through SOCE.[9,10] Because myocardial STIM1 expression undergoes marked downregulation during early postnatal development, its role in adult heart physiology has been questioned.[9] Nonetheless, the reemergence of STIM1-mediated SOCE in response to pro-hypertrophic stimuli in-vitro or pressure overload in vivo suggests its active participation in the development and progression of adverse cardiac remodeling in response to stress. Indeed, STIM1 and SOCE were shown to be critical mediators of pathological cardiac hypertrophy.[1,10,11] Furthermore, exogenous STIM1 overexpression accelerated disease progression likely by increasing sarcoplasmic reticulum (SR) Ca^{2+} leak and the frequency of ryanodin receptor type 2 (RYR2)–dependent Ca^{2+} sparks and waves.[12]

While STIM1 overexpression clearly exacerbates pathological hypertrophy, its depletion is associated with worsening not amelioration of cardiac dysfunction. Specifically, multiple groups have demonstrated adverse cardiac remodeling in global haploinsufficient STIM1 mice and cardiac-restricted STIM1 knockouts.[13,14] Moreover, using AAV9 (adeno-associated virus serotype 9)-mediated gene delivery of a short hairpin RNA directed against STIM1 (AAV9-shSTIM1), our group has documented the abrogation of compensated cardiac hypertrophy in response to pressure overload at the expense of acceleration and worsening of the heart failure phenotype.[10,15] The apparently discrepant results garnered from studies in which STIM1 is overexpressed or depleted have raised fundamental questions regarding the role of cardiomyocyte STIM1 in the regulation of normal and abnormal cardiac function at baseline and in response to stress.[10,15]

Beyond the canonical SOCE-dependent pathway by which STIM1 is believed to modulate cardiac function, a de novo SOCE-independent property of STIM1 has also emerged in recent years.[16] Specifically, Zhao et al[16] elegantly demonstrated in STIM1 overexpressing rat ventricular myocytes, an increase in SR Ca^{2+} content due to direct binding of STIM1 to the SERCA2a (sarco/endoplasmic reticulum ATPase 2a)-regulatory protein phospholamban. These intriguing data highlighted an entirely new paradigm by which STIM1 can regulate intracellular Ca^{2+} cycling and excitation-contraction coupling in a SOCE-independent manner, re-invigorating the debate over its role in the adult heart in which SOCE is normally absent.[17,18] Moreover, STIM1 expression which is enriched in cardiac pacemaker cells, appears to regulate sinus rate, since STIM1 silencing promoted sinoatrial dysfunction and bradycardia in vivo.[19–21]

In light of these findings, we hypothesized that STIM1 may play a central role in the regulation of electrophysiological function and arrhythmias in the adult heart. To address this hypothesis, we generated a novel inducible cardiomyocyte-specific STIM1-KD (STIM1 knockdown) strategy using an αMHC (α-myosin heavy chain)-MerCreMer system. We report an unexpectedly high mortality rate in vivo as well as high propensity for rapid pacing-induced ventricular tachycardia/fibrillation (VT/VF) secondary to the pathogenesis of spatially discordant action potential duration (APD) alternans, ex vivo. Our findings highlight a direct role for STIM1 depletion in these electrical abnormalities.

METHODS

All the data that support the findings of this study are available from the corresponding author on reasonable request. All experimental procedures complied with the National Institutes of Health Guide for the Care and Use of Laboratory Animals. Protocols were approved by the Institutional Animal Care and Use Committee of the Icahn

School of Medicine at Mount Sinai. All mice were on a C57Bl/6 background. Mice had unlimited access to standard food and water and were housed in an environment in which a 12 h/12 h light/dark cycle was maintained.

Cardiomyocyte-Specific STIM1-KD Mouse Model

STIM1-KD mice were generated by crossing homozygous STIM1$^{fl/fl}$ mice, in which exon 2 of STIM1 was floxed by 2 loxP sites, with cardiomyocyte-specific αMHC-Cre$^{tg/-}$ mice.[22] At 4 weeks of age, mice were weaned, ear-tagged, and a sample of tail tissue was collected for subsequent genotyping. Tissue samples were analyzed at TransnetYX (Cordova, TN) to determine the STIM1 genotype as well as the expression of the αMHC-Cre transgene. Control (STIM1-Ctl) and STIM1-KD mice refer to STIM1$^{flox/flox}$/αMHC-Cre$^{-/-}$ and STIM1$^{flox/flox}$/αMHC-Cre$^{tg/-}$, respectively. Cre-Ctl refers to αMHC-Cre$^{tg/-}$ mice, which served as an additional control.

Tamoxifen Preparation and Administration

Tamoxifen (Sigma-Aldrich, T5648) was dissolved in peanut oil (Sigma-Aldrich, P2144) at 10 mg/mL by shaking for 4 hours at room temperature. Once in solution, tamoxifen was shielded from light and stored at −20°C. Fresh solutions were prepared weekly. Adult (10–14 weeks of age) STIM1$^{fl/fl}$/αMHC-Cre$^{tg/-}$ (STIM1-KD), STIM1$^{fl/fl}$/αMHC-Cre$^{-/-}$ (STIM1-Ctl), and αMHC-Cre$^{tg/-}$ (Cre-Ctl) mice were injected intraperitoneally on 5 consecutive days with tamoxifen (60 mg/kg per day). Experiments were conducted 8 days after the first tamoxifen injection.

Echocardiography

Echocardiography was performed in conscious mice under light sedation with an intraperitoneal injection of 75 mg/kg ketamine. Short-axis parasternal views were obtained using a 13MHz GE-i13L probe as recommended by the American Society of Echocardiography. M-mode and 2D images were obtained at the left ventricular (LV) mid-papillary level from the parasternal short-axis views. The transducer position was carefully adjusted until the short-axis image of the LV cavity appeared to be circular, indicating perpendicular intersection of the ultrasonic beam with the long axis of the LV. LV wall thickness and cavity dimensions were measured in systole and diastole with M-mode echocardiography. Fractional shortening corresponding to the ratio of change in LV diameter between the relaxed and contracted states, was used as an index of LV performance, using the following formula: Fractional shortening=(left ventricular internal dimension during diastole–left ventricular internal dimension during systole)/left ventricular internal dimension during diastole.

Cardiomyocyte Isolation

Cardiomyocytes were isolated from STIM1-Ctl, Cre-Ctl, and STIM1-KD hearts. The heart was rapidly excised from the chest and Langendorff-perfused. Tyrodes solution (137 mmol/L NaCl, 5.4 mmol/L KCl, 1 mmol/L $MgCl_2$, 10 mmol/L glucose, 10 mmol/L HEPES [pH 7.4], 10 mmol/L 2,3-butanedione monoxime, and 5 mmol/L taurine, and oxygenated with 100% O_2) was maintained at 37°C and retrogradely perfused through the aorta. The enzymatic digestion was initiated by adding collagenase type B (300 U/mL; Worthington) and hyaluronidase (0.1 mg/mL; Worthington) to the perfusion solution for 20 minutes. LV tissue was isolated, and the digestion was stopped by bathing the LV in a solution of Tyrodes containing 1% BSA. Digested LV tissue was manually dissociated by gentle repeated flushing to physically separate the cells. The cell suspension was filtered through a cell strainer (100 μm pore size; BD Falcon) and gently centrifuged at 500 rpm for 1 minute. The pellet containing the myocyte fraction was frozen for Western blot studies.

Western Blot

Western blots were performed using 4% to 20% tris-glycine gels (BioRad). Fifteen micrograms of protein was loaded. Primary antibodies against β-Actin (Santa Cruz), STIM1 (Sigma-Aldrich), Cx43 (Sigma), Phospho-Cx43 pSer368 (Milipore), Phospho-CAMKII (phosphorylated Ca^{2+}/calmodulin-dependent protein kinase II) at pThr286 (Thermo), and Nav1.5 (Alomone) were used. Secondary antibodies were species-specific horseradish peroxidase-conjugated antibodies (Thermo Scientific).

Quantitative Polymerase Chain Reaction

After RNA extraction and cDNA synthesis, quantitative real-time polymerase chain reaction was performed with SYBR-green-based detection of double-stranded DNA (Applied Bioscience). Results were expressed in absolute units of mRNA expression for STIM1-Ctl and STIM1-KD calculated using the $2^{-\Delta\Delta Ct}$ method. mRNA levels of each target gene were normalized to those of the internal control, GAPDH. The following primers were used in this study: GAPDH (forward 5′-ggcaaagtggagattgttgc-3′; reverse 5′-aatttgccgtgagtggagtc-3′), Cx43 (forward 5′-ccacggagaaaaccatcttc-3′; reverse 5′-aaggatcgcttcttcccttc-3′), Nav1.5 (forward 5′-tcttcgacagcatcatcgtc-3′; reverse 5′-gatttggccagcttgaagac-3′), KV1.4 (forward 5′-tgttgagtttgcctctgctg-3′; reverse 5′-tcatggacccacagacaatg-3′), KV4.2 (forward 5′-tgtgtctgcacgtgacaatg-3′; reverse 5′-gtggtggcttggaatgaac-3′), KV4.3 (forward 5′- ttcccccatttgagtctgag-3′; reverse 5′-tccccatcaataccctgag-3′), and KCHIP2 (potassium channel interacting protein 2; forward 5′- tcagtgattcttcggggaac-3′; reverse 5′-tcgtgatacagccatccttg-3′).

Optical Action Potential Mapping of Ex Vivo Perfused Hearts

Hearts were excised rapidly and perfused on a Langendorff apparatus with Tyrode's solution containing 114 mmol/L NaCl, 25 mmol/L $NaHCO_3$, 4.6 mmol/L KCl, 1.5 mmol/L $CaCl_2$, 1.2 mmol/L Na_2PO_3, 0.7 mmol/L $MgCl_2$, and 10 mmol/L Glucose (pH 7.40; 95% O2/5% CO2). Perfusion pressure was maintained at 60 to 70 mm Hg by regulating coronary perfusion flow throughout the experiment. Preparations were positioned in a custom-built tissue bath and pressed gently against a glass imaging window using a stabilizing piston.[23–25] Movement was minimized by

perfusion with blebbistatin (10 mmol/l) for 10 to 15 minutes. To avoid surface cooling, preparations were immersed in the coronary effluent maintained at a physiological temperature by a heat exchanger assembly. Hearts were stimulated with a pacing electrode placed on the anterior epicardial surface of the LV mid-way between apex and base. Cardiac rhythm was monitored continuously with silver electrodes connected to an ECG amplifier.

Optical action potentials were measured with an 80×80-pixel charge-coupled device camera coupled to an imaging macroscope that contained a high numerical aperture lens, a dichroic mirror, excitation and emission filters, a beam splitter, and a light-collimating tube. Excitation light was provided by a low-noise, high-power tungsten-halogen lamp and directed in an epifluorescence configuration onto the heart through a side port of the macroscope in a manner that minimized heterogeneity of the incident light across the mapped region. Emitted light was collected by the front lens of the macroscope, filtered, and directed onto the charge-coupled device detector. High-resolution optical action potentials were measured simultaneously from 6400 sites at 1 ms temporal resolution during each recording. To improve signal quality, spatial binning was performed, which yielded an array of 400 (20×20) high-fidelity optical action potentials that were amenable to accurate automated analyses.

Ex Vivo Experimental Protocol

As illustrated below, the experimental protocol consisted of pacing hearts at progressively shorter pacing cycle lengths (PCL) starting at 140 ms and in decrements of 10 ms up to PCL 50 ms or onset of sustained VT/VF. At each PCL, the stimulus train had a duration of at least 1 minute. During the initial (steady-state) phase of the pacing protocol (140–90 ms), we found no evidence of beat-to-beat variability. Hence, steady-state APD and conduction velocity (CV) values were determined over that range. Alternans were clearly evident in most STIM1-KD hearts by PCL 70 ms. No sustained arrhythmias were ever encountered at PCL >60 ms. Recordings were typically performed before and after the end of the pacing train.

PCL (ms)	140	120	100	90	70	60	50
Protocol:	Steady State—APD/CV measurements				Alternans	VT/VF Zone	

Conduction Velocity

Conduction delays were assessed by recording action potentials during steady-state pacing. Local activation time at each site was defined as the maximum first derivative during the upstroke of the action potential. Velocity vectors (magnitude and direction) were derived from the activation times of each pixel relative to those of its neighbors. CV was measured by averaging the magnitude of the velocity vectors.

APD Heterogeneity and APD Alternans

Repolarization times at 75% relative to the action potential amplitude were quantified. APD was defined as the temporal difference between the repolarization and activation times at each site. APD heterogeneity was calculated as the SD of all simultaneously measured APD values (from N=200 spatially binned voxels) across the epicardial surface in each recording. Action potential alternans was quantified as the average difference in APD between 3 consecutive pairs of odd and even beats (ΔAPD) at a PCL of 140 ms (negative control baseline rate) and 70 ms representing the fast rate before onset of arrhythmias.

Phase Mapping

The phase transformation allows tracking of cardiac activity by defining relative timing of events along the action potential, independently of the amplitude of the instantaneous signal. The Hilbert transformation consists of applying the Hilbert operator on the voltage-time series $V(t)$ to return a phase-shifted function $V_{HT}(t)$ in the same domain. This approach, which was initially described by Bray and Wikswo,[26] is now generally used in phase mapping studies.[27] The phase $\theta(t)$ of a time-dependent function represents its periodic behavior over time and is computed as follows:

$$\theta(t) = \tan^{-1}\left[V_{HT}(t) / V(t)\right]$$

where $V(t)$ is the measured epicardial voltage, $V_{HT}(t)$ is the phase-shifted function using the Hilbert transformation; and $\tan^{-1}$ indicates the inverse of the tangent function.

Statistical Analyses

Electrophysiological measurements performed at the terminal time point of the study are expressed as mean±SEM. Differences between groups were evaluated by using χ^2 testing for discrete variables (eg, presence versus absence of VT/VF). For continuous variables, the Student t test or ANOVA were performed. The unpaired Student t test was used to compare differences between 2 groups. For multiple comparisons, 2-way ANOVA followed by Sidak's multiple comparisons test was used. $P<0.05$ was considered significant. Echocardiographic measurements were performed on multiple days (day 1, day 3, day 5, and day 8) in each group to define the time-course of hemodynamic changes. For those analyses, 2-way ANOVA followed by Sidak's or Tukey's multiple comparisons testing within and across outcomes were performed. An alpha level of 0.001 was used to establish significance.

RESULTS

Cardiomyocyte-Specific STIM1 Depletion in the Adult Heart Promotes Adverse Remodeling

To examine the role of cardiomyocyte STIM1 expression in the adult murine heart, we performed constitutive cardiomyocyte-restricted tamoxifen-inducible knockdown of STIM1 (STIM1-KD) using a cre-loxP system. The cardiomyocyte-specific nature of our STIM1-KD strategy is shown in Figure 1. While robust (>80%, $P<0.0001$) STIM1 downregulation was evident in protein lysates from isolated cardiomyocytes of STIM1-KD versus STIM1-Ctl hearts, STIM1 levels were comparable ($P=0.47$) when

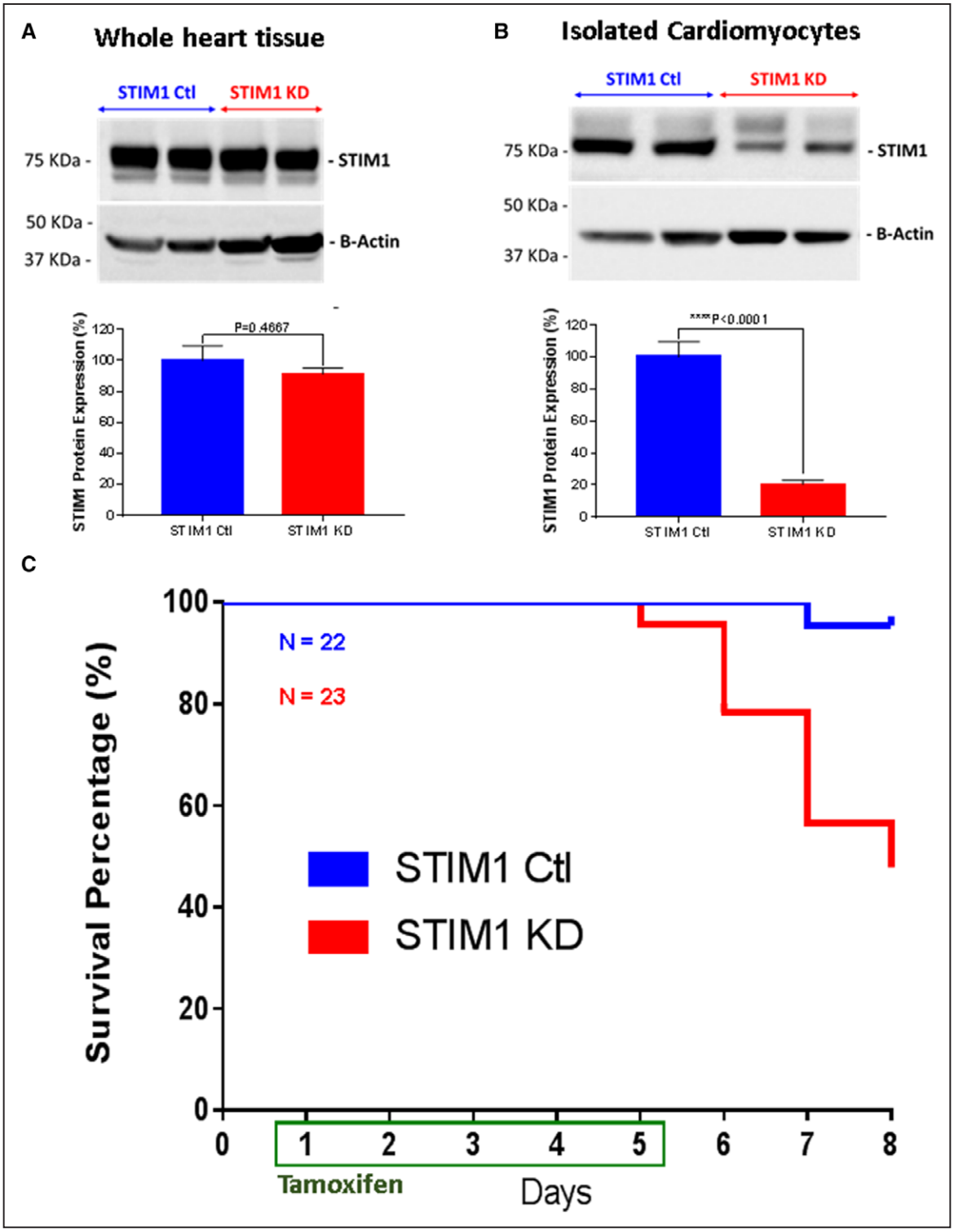

Figure 1. Inducible, cardiomyocyte-specific STIM1 (stromal interaction molecule 1) knockdown model.
Representative Western blot and quantification of STIM1 protein expression on whole heart tissue (**A**) and isolated cardiomyocytes (**B**) on day 8 after initial tamoxifen injection. Statistical test: Mann-Whitney unpaired *t* test shows NS (*P*=0.4667) on heart lysates (n=6/group) and ****P*<0.0001 on isolated cardiomyocytes (n=6 and n=7 respectively for STIM1-Ctl [control] and STIM1-KD [knock-down]). **C**, Survival curve of STIM1-Ctl (blue line) and STIM1-KD mice (red line), from day 1 to day 8. Tamoxifen injection was performed from day 1 to day 5 (green rectangle). n=22 and 23 respectively for STIM1-Ctl and STIM1-KD mice.

measured in whole heart tissues from the 2 groups (Figure 1A and 1B). The first major unexpected outcome of our cardiomyocyte-restricted STIM1-KD model is shown in Figure 1C. Specifically, these mice exhibited very poor survival with an overall mortality rate reaching >50% within only 8-days after the initiation of the tamoxifen regimen

compared with STIM1-Ctl (Figure 1C). To exclude potential artefactual effects associated with the use of tamoxifen specifically on the *Cre-recombinase* background (present in STIM1-KD but not in STIM1-Ctl mice), we used an additional set of heterozygous Mer-Cre-Mer mice (Cre-Ctl) as a second control for the presence of Cre but without cardiomyocyte STIM1 depletion. As with STIM1-Ctl, the identical tamoxifen regimen did not impact survival rate of Cre-Ctl mice (Figure IA in the Data Supplement), reaffirming the importance of cardiomyocyte STIM1 downregulation per se in the poor survival of adult mice.

We next investigated whether the rise in mortality in STIM1-KD mice was a consequence of adverse structural and mechanical remodeling leading to pump failure. To that end, cardiac function was assessed by echocardiography in STIM1-KD, STIM1-Ctl, and Cre-Ctl mice (Figure 2 and Table 1). During the 8-day course of the experiment, STIM1-KD and Cre-Ctl but not STIM1-Ctl mice exhibited a modest decrease in heart rate. On day 8, the average heart rates of STIM1-KD and Cre-Ctl mice were ≈10% lower (P<0.01) than that of STIM1-Ctl mice (Figure 2B). More importantly, fractional shortening (FS) progressively decreased from ≈60% to 20% in STIM1-KD and Cre-Ctl but not STIM1-Ctl mice (Figure 2C). Concomitant with the development of LV dysfunction, echocardiographic measurements on day 8 revealed a marked rise in the LV internal diameter during systole and diastole (Figure 2D), as well as a decrease in the interventricular septal dimension (Figure 2E) and LV posterior wall thickness during systole and diastole (Figure 2F) in STIM1-KD and Cre-Ctl hearts. Because STIM1-KD and Cre-Ctrl mice exhibited comparable LV dysfunction by the tamoxifen regimen, the early mortality seen exclusively in the former group was not likely caused, at least exclusively, by pump failure.

As mentioned above, STIM1-KD mice exhibited an unexpected mortality rate that reached >50% after only 8 days of cardiomyocyte-restricted STIM1 depletion. We speculated that a component of the accelerated mortality rate is caused by ventricular arrhythmias driven primarily by cardiomyocyte STIM1 depletion. STIM1, which is known to impact cellular function upon store depletion, has been shown to affect SR Ca^{2+} cycling in myocytes. We, therefore, hypothesized that challenge with rapid stimulus trains which promote cytosolic Ca^{2+} overload would unmask the potential arrhythmic susceptibility of STIM1-KD hearts. Therefore, we assessed the susceptibility of hearts from each group to 1-minute rapid stimulus trains (PCL 60 ms and 50 ms). Indeed, STIM1-KD hearts exhibited clear propensity to pacing-induced arrhythmic activity. Shown in Figure 3A are representative action potential traces that illustrate the range of arrhythmic responses observed in these hearts. Of particular relevance to sudden death, STIM1-KD hearts also exhibited increased incidence of sustained VT/VF in response to rapid stimulation compared with STIM1-Ctl and Cre-Ctl hearts (44% STIM1-KD versus 8.4% STIM1-Ctl and 11.1% Cre-Ctl, Figure 3B).

Cardiomyocyte-Specific STIM1 Depletion in the Adult Heart Alters Basal Electrophysiological Properties

Next, we investigated the electrophysiological substrate of STIM1-KD hearts relative to their STIM1-Ctl counterparts. We began by determining whether myocardial CV is altered in these mice. As demonstrated in Figure 4A, average CV in STIM1-KD hearts (red) was significantly decreased relative to their STIM1-Ctl counterparts (blue) at PCL <140 ms. Of note, differences in CV between the 2 groups were exacerbated as PCL was reduced reflecting rate-dependent conduction slowing in STIM1-KD but not STIM-Ctl hearts (Figure 4A). Representative isochrone maps depicting myocardial conduction in STIM1-Ctl and STIM1-KD hearts are shown in Figure 4B. Conduction differences were related to the loss of cardiomyocyte STIM1 per se, as CV was comparable in STIM1-Ctl and Cre-Ctl hearts (Figure IB in the Data Supplement). To gain insight into whether CV slowing was sufficient to explain the heightened propensity of STIM1-KD hearts to arrhythmias, we compared CV in hearts that were prone to VT/VF versus those that were not and found no differences (P=0.99, NS) between the 2 groups (Figure 4C). Nonetheless, we proceeded to investigate the putative molecular mechanisms underlying CV slowing in STIM1-KD hearts. We began by measuring the expression of the total and phosphorylated (at Ser368) components of the main ventricular gap junction protein, Cx43. While total Cx43 expression was comparable in STIM1-KD and STIM1-Ctl hearts, the Ser368 phosphorylated component was markedly increased in the STIM1-KD group as reflected by the increased pCx43/Cx43 ratio (Figure 4D). We next measured the expression of the alpha subunit of the fast inward Na channels (Nav1.5) that mediate the upstroke of the action potential. Paradoxically, we found an increase in Nav1.5 protein expression in STIM1-KD hearts discounting a role for altered Na channel alpha-subunit expression in the CV slowing that we observed (Figure 4E). Since CV slowing in STIM1-KD hearts was rate-dependent in nature, we speculated that a change in Na channel function may be implicated. Therefore, we measured the expression of the pCAMKII (phosphoactive component of CAMKII) which is known to modulate Na channel availability in a rate-dependent manner. As shown in Figure 4F, pCAMKII expression was markedly increased in STIM1-KD likely contributing to the rate-dependent CV slowing that we observed in these hearts.

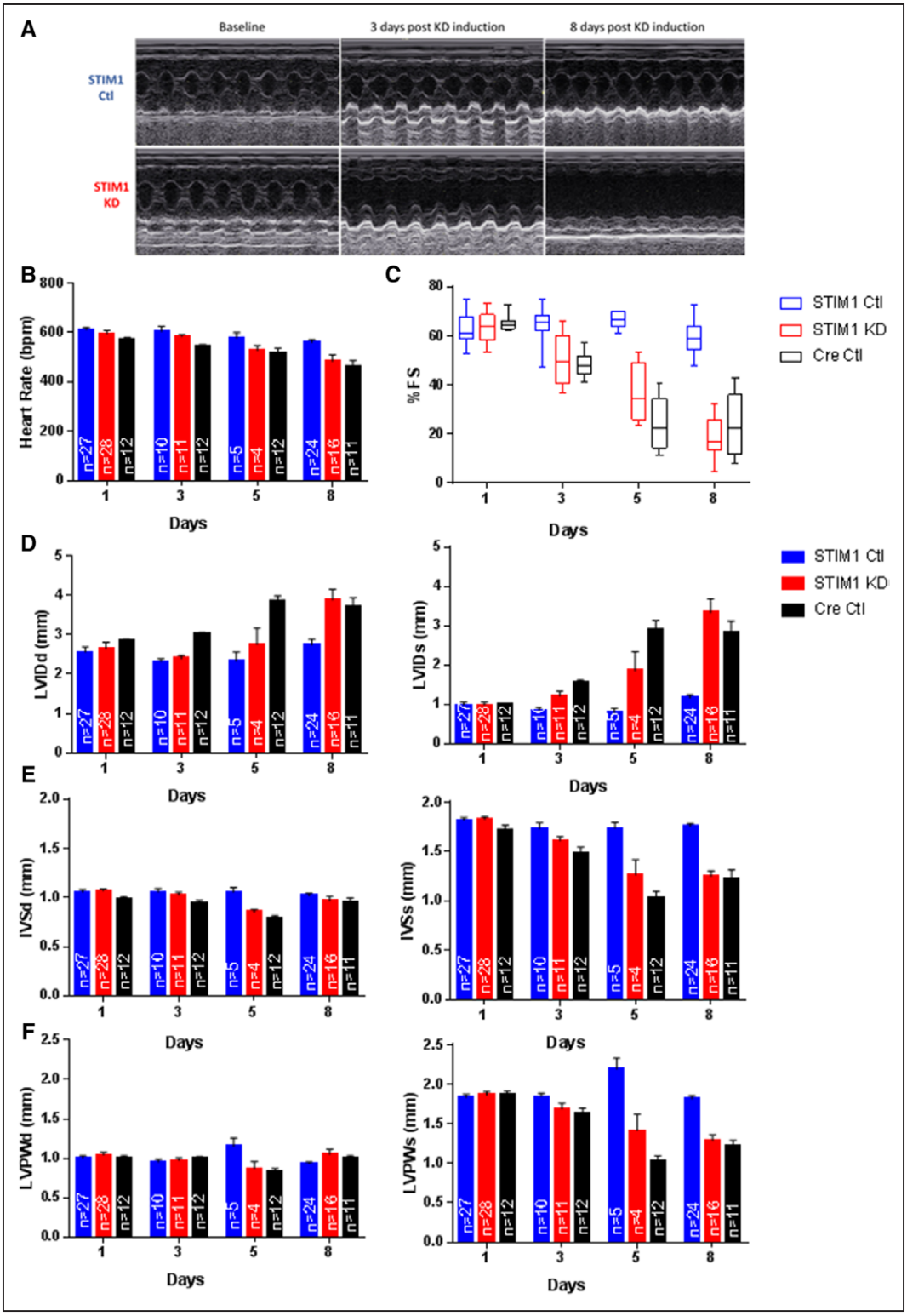

Figure 2. Cardiac remodeling of adult STIM1-KD (stromal interaction molecule 1 knockdown) mice.
Echocardiographic (echo) measurements at baseline (day 1), 3, 5, and 8 days after the first tamoxifen injection in STIM1-Ctl (control), STIM1-KD, and Cre-Ctl mice. **A**, Representative echo images of STIM1-Ctl and STIM1-KD mice at baseline and days 5 and 8 after the first tamoxifen injection. Different parameters were measured by echo: (**B**) heart rate, (**C**) percentage of cardiac fractional shortening (%FS), (**D**) left ventricular internal diameter during systole (LVIDs) and diastole (LVIDd), (**E**) interventricular septum thickness during systole (IVSs) and diastole (IVSd), and (**F**) left ventricular posterior wall thickness during systole (LVPWs) and diastole (LVPWd). The number of animal is embedded in the bar graphs for each time point (n). Statistics for echo parameters are summarized in Table 1.

Table 1. Statistical Analyses on Echocardiographic Parameters

	Heart Rate	%FS	LVIDs	LVIDd	IVSs	IVSd	LVPWs	LVPWd
2-Way ANOVA-Sidak's multiple comparisons test								
STIM1-Ctl vs STIM1-KD								
Day 1	NS	NS	NS	NS	NS	NS	NS	NS
Day 3	NS	*P*<0.0005	NS	NS	NS	NS	NS	NS
Day 5	NS	*P*<0.0001	NS	NS	*P*<0.0024	NS	*P*<0.0001	NS
Day 8	NS	*P*<0.0001	*P*<0.0001	*P*<0.0001	*P*<0.0001	NS	*P*<0.0001	NS
STIM1-Ctl vs Cre-Ctl								
Day 1	NS	NS	NS	NS	NS	NS	NS	NS
Day 3	NS	*P*<0.0001	NS	NS	*P*<0.001	NS	NS	NS
Day 5	NS	*P*<0.0001	*P*<0.0001	*P*<0.001	*P*<0.0001	*P*<0.001	*P*<0.0001	*P*<0.002
Day 8	*P*<0.002	*P*<0.0001	*P*<0.0001	*P*<0.002	*P*<0.0001	NS	*P*<0.0001	NS
STIM1-KD vs Cre-Ctl								
Day 1	NS	NS	NS	NS	NS	NS	NS	NS
Day 3	NS	NS	NS	NS	NS	NS	NS	NS
Day 5	NS	NS	NS	NS	NS	NS	NS	NS
Day 8	NS	NS	NS	NS	NS	NS	NS	NS
2-Way ANOVA-Tukey's multiple comparisons test								
STIM1-Ctl								
Day 1 vs 3	NS	NS	NS	NS	NS	NS	NS	NS
Day 1 vs 5	NS	NS	NS	NS	NS	NS	NS	NS
Day 1 vs 8	NS	NS	NS	NS	NS	NS	NS	NS
Day 3 vs 5	NS	NS	NS	NS	NS	NS	NS	NS
Day 3 vs 8	NS	NS	NS	NS	NS	NS	NS	NS
Day 5 vs 8	NS	NS	NS	NS	NS	NS	NS	NS
STIM1-KD								
Day 1 vs 3	NS	*P*<0.0001	NS	NS	*P*<0.01	NS	NS	NS
Day 1 vs 5	NS	*P*<0.0001	NS	NS	*P*<0.0001	*P*<0.01	*P*<0.003	NS
Day 1 vs 8	*P*<0.0001	*P*<0.0001	*P*<0.0001	*P*<0.0001	*P*<0.0001	NS	*P*<0.0001	NS
Day 3 vs 5	NS	*P*<0.01	NS	NS	*P*<0.01	NS	NS	NS
Day 3 vs 8	*P*<0.0005	*P*<0.0001	*P*<0.0001	*P*<0.0001	*P*<0.0001	NS	*P*<0.0001	NS
Day 5 vs 8	NS	*P*<0.0003	*P*<0.0005	NS	NS	NS	NS	NS
Cre-Ctl								
Day 1 vs 3	NS	*P*<0.0001	NS	NS	NS	NS	NS	NS
Day 1 vs 5	NS	*P*<0.0001	*P*<0.0001	*P*<0.003	*P*<0.0001	*P*<0.002	*P*<0.0001	NS
Day 1 vs 8	*P*<0.0003	*P*<0.0001	*P*<0.0001	NS	*P*<0.0001	NS	*P*<0.0001	NS
Day 3 vs 5	NS	*P*<0.0001	*P*<0.0001	NS	*P*<0.0001	NS	*P*<0.0001	NS
Day 3 vs 8	*P*<0.01	*P*<0.0001	*P*<0.0001	NS	*P*<0.005	NS	*P*<0.0002	NS
Day 5 vs 8	NS	NS	NS	NS	NS	NS	NS	NS

Ctl indicates control; FS, fractional shortening; IVSs, intraventricular septum diameter in systole; IVSd, intraventricular septum diameter in diastole; KD, knockdown; LVIDd, left ventricular internal dimension during diastole; LVIDs, left ventricular internal dimension during systole; LVPWd, left ventricular posterior wall dimension in diastole; LVPWs, left ventricular posterior wall dimension in systole; and STIM1, stromal interaction molecule 1.

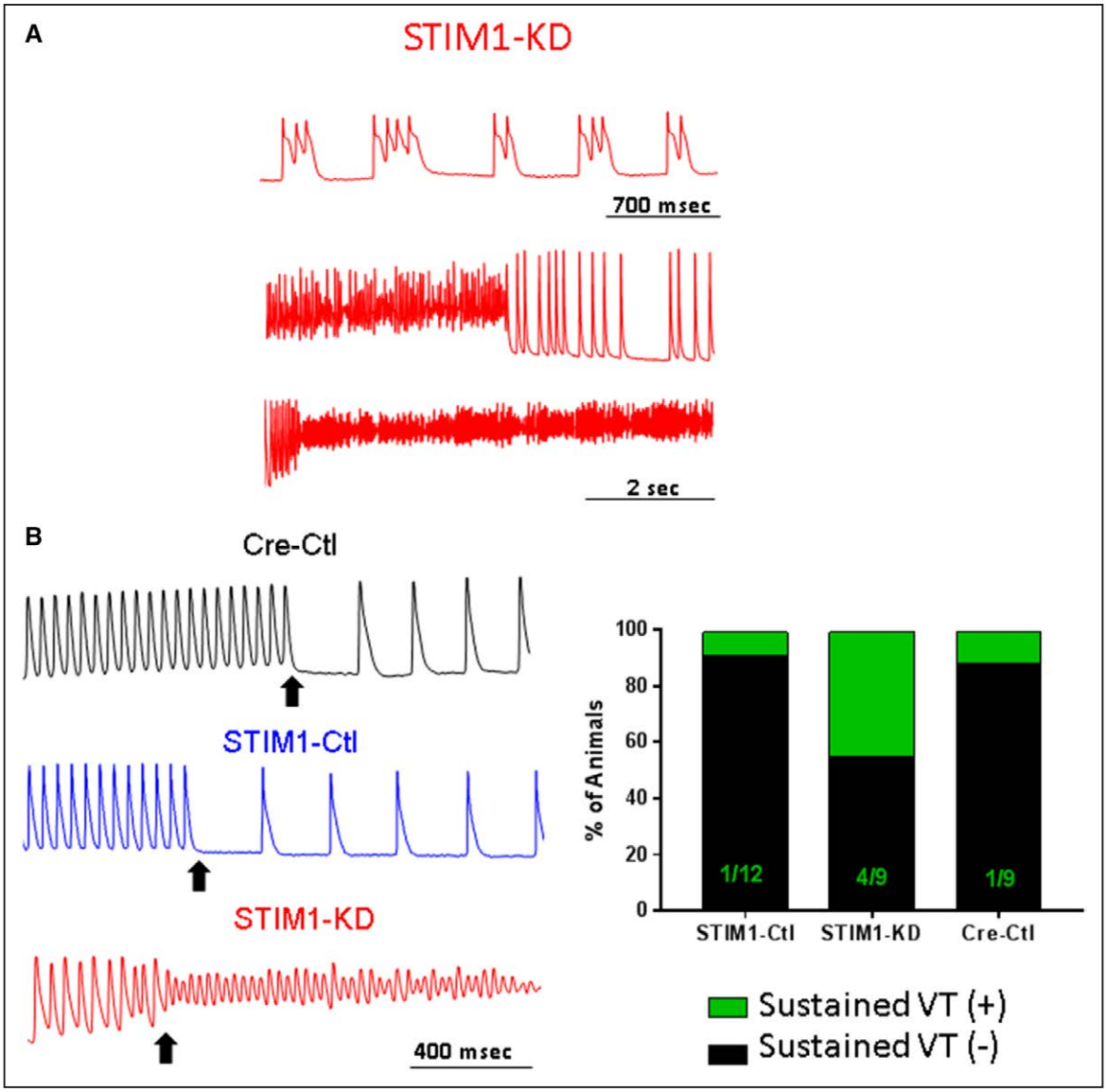

Figure 3. Arrhythmia susceptibility of STIM1-KD (stromal interaction molecule 1 knockdown) hearts.
A, Representative action potential traces recorded from STIM-KD hearts after challenge with rapid stimulation. Action potentials document a wide range of arrhythmic activity from frequent after depolarizations to nonsustained and sustained ventricular tachycardia/ventricular fibrillation (VT/VF). **B**, **Left**, Representative action potential traces from Cre-Ctl (Cre-recombinase–control), STIM1-Ctl, and STIM1-KD hearts recorded during and immediately after the cessation of the rapid stimulus train (marked by black arrow). Note presence of action potential alternans before onset of VT/VF in STIM1-KD heart. **Right**, Incidence of VT/VF in all groups.

In addition to myocardial conduction slowing, APD prolongation is a standard index of electrophysiological remodeling in hypertrophy and heart failure. Despite a trend towards longer average APD values in STIM1-KD hearts relative to STIM1-Ctl, differences did not reach statistical significance at any of the tested PCLs (Figure 5A). In contrast, APD heterogeneity indexed by the SD of APD values measured simultaneously from 200 loci across a 4×4 mm2 region of the epicardial surface was increased (Figure 5B). Once again, this change was likely related to the loss of cardiomyocyte STIM1 expression as APD heterogeneity was comparable in STIM1-Ctl and Cre-Ctl hearts (Figure IC in the Data Supplement). Similar to CV slowing, APD heterogeneity was also comparable (P=0.34, NS) in STIM1-KD hearts that were prone to VT/VF versus those that were not (Figure 5C). Analysis of K-channel expression with a focus on the molecular determinants of the transient outward K current as the predominant repolarizing force in mice, revealed increased Kv1.4 levels at the expense of decreased Kv4.2, Kv4.3, and KChIP2 expression in STIM1-KD versus STIM1-Ctl hearts (Figure 5D).

Cardiomyocyte-Specific STIM1 Depletion in the Adult Heart Promotes the Development of Discordant Action Potential Alternans

A key observation from Figure 3A was that the initiation of sustained VT/VF in STIM1-KD hearts was preceded

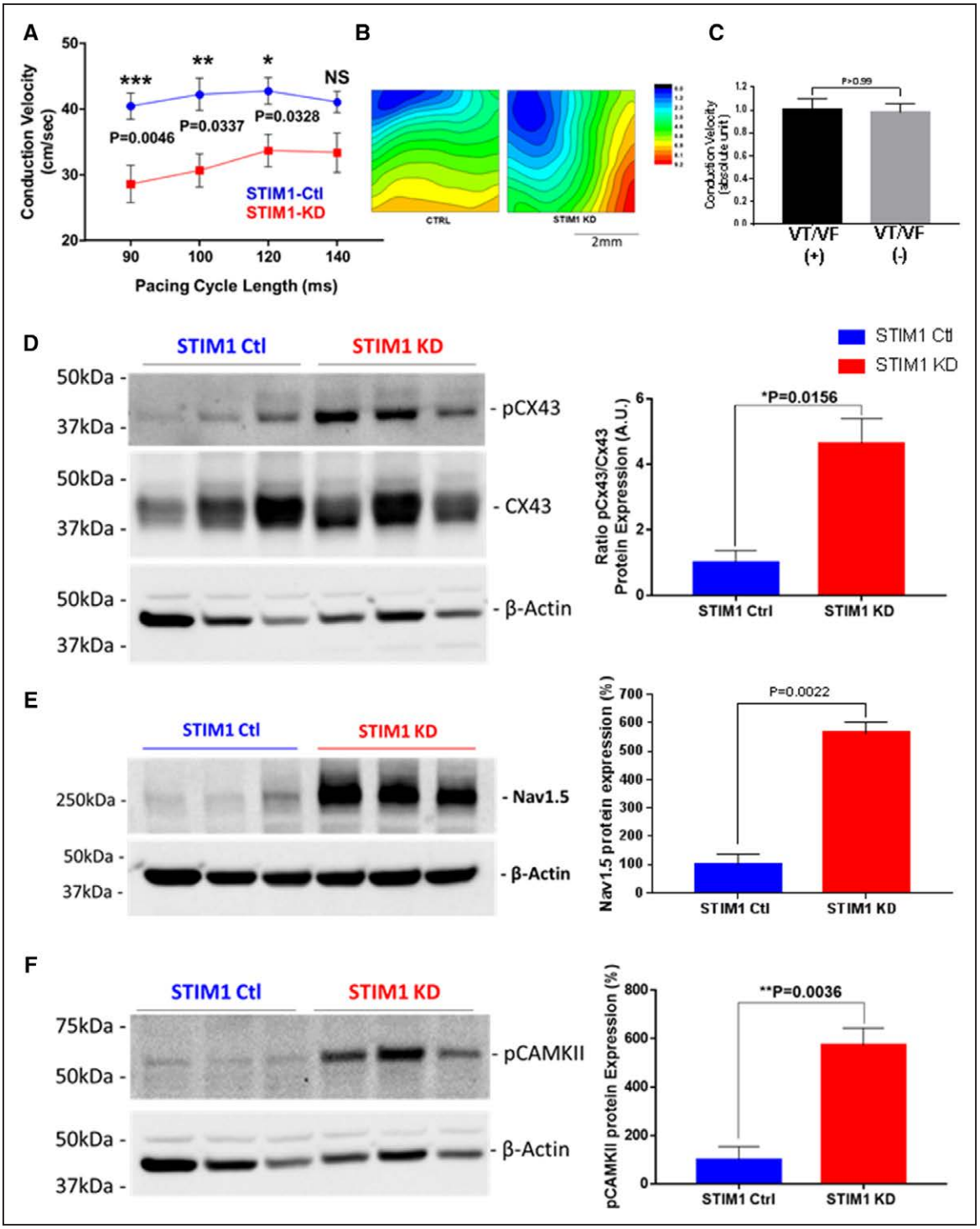

Figure 4. Electrophysiological remodeling in STIM1-KD (stromal interaction molecule 1 knockdown) hearts.
Langendorff-perfused hearts from STIM1-KD and STIM1-Ctl (control) mice were loaded with the voltage–sensitive dye, di-4-ANEPPS and paced from the left ventricular at pacing cycle lengths (PCLs) from 140 to 90 ms in 10 ms decrements. **A**, Conduction velocity (CV) was plotted against PCL. Statistics: STIM1-KD (n=7) vs STIM1-Ctl (n=9), 2-way ANOVA followed by Sidak's multiple comparison test. **B**, Representative depolarization isochrone maps recorded at PCL 140 ms for STIM1-Ctl and STIM1-KD hearts. **C**, Comparison of average CV in ventricular tachycardia/ventricular fibrillation (VT/VF) (+) vs VT/VF (–) STIM1-KD hearts. **D**, Representative western blot of Cx43 and phospho-Cx43 (pSer368) protein expression in STIM1-Ctl (n=6) and STIM1-KD hearts (n=7) and quantification of the protein expression ratio. **E**, Representative western blot of Nav1.5 protein in STIM1-Ctl (n=6) and STIM1-KD hearts (n=7) and quantification of the protein expression. **F**, Representative western blot of phospho-CAMKII (pThr286) protein in STIM1-Ctl (n=6) an STIM1-KD hearts (n=7) and quantification of the protein expression. Statistical analysis using the unpaired *t* test. *P* value displayed on each bar graph. Data presented as mean ±SEM.

by a clear pattern of action potential alternans. Therefore, we set out to formally investigate this parameter, which we and others have mechanistically linked to the pathogenesis of VT/VF. Indeed, as shown in Figure 6A, progressive elevation in pacing rate (reduction in PCL) unmasked action potential alternans that grew in ampli-

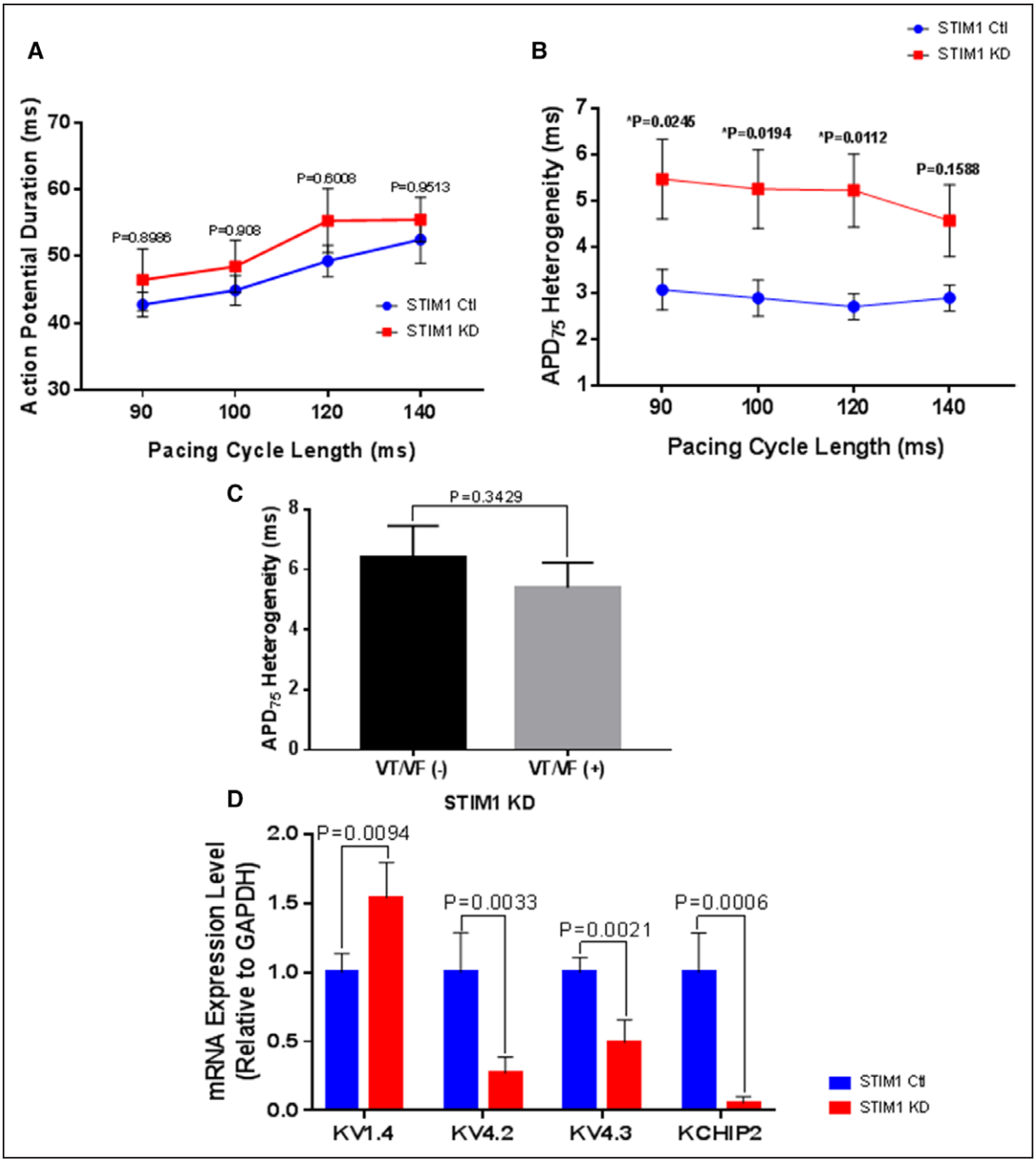

Figure 5. Expression of molecular determinants of conduction in STIM1-Ctl (stromal interaction molecule 1 control) and STIM1-KD (knockdown) hearts.

A, Average steady-state action potential duration (APD_{75}) values measured over a range of pacing cycle length (PCL). Analysis is based on 7 STIM1-KD and 9 STIM1-Ctl hearts. **B**, Range of APD_{75} values measured across the mapping field as an index of APD heterogeneity. Analysis is based on 6 STIM1-KD and 7 STIM1-Ctl mice. **C**, Comparison of APD_{75} heterogeneity in ventricular tachycardia/ventricular fibrillation (VT/VF) (+) vs VT/VF (–) STIM1-KD hearts. **D**, mRNA expression of K-channel subunits: Kv1.4, Kv4.2, Kv4.3, and KCHIP2 in STIM1-Ctl and STIM1-KD hearts (n=4/group). Statistical analysis using the unpaired *t* test. Data presented as mean±SEM.

tude before onset of VT/VF in STIM1-KD hearts. The magnitude of alternans was quantified by measuring the difference in APD_{75} between odd and even beats (ΔAPD_{75}) during steady-state pacing at basal (PCL 140 ms as a negative control) and rapid (PCL 70 ms) pacing. While the magnitude of APD alternans was minimal in both groups at PCL 140 ms, it underwent a marked increase at PCL 70 ms exclusively in STIM1-KD hearts (Figure 6B and 6C, and Table 2). No difference in alternans magnitude was observed between STIM1-Ctl and Cre-Ctl hearts (Figure ID in the Data Supplement). To determine whether the pathogenesis of action potential alternans in STIM1-KD hearts was mechanistically linked to their intrinsic vulnerability to VT/VF, we compared ΔAPD_{75} (APD alternans) in VT/VF(+) and VT/VF(–) STIM1-KD hearts. Indeed, the subset of STIM1-KD hearts that

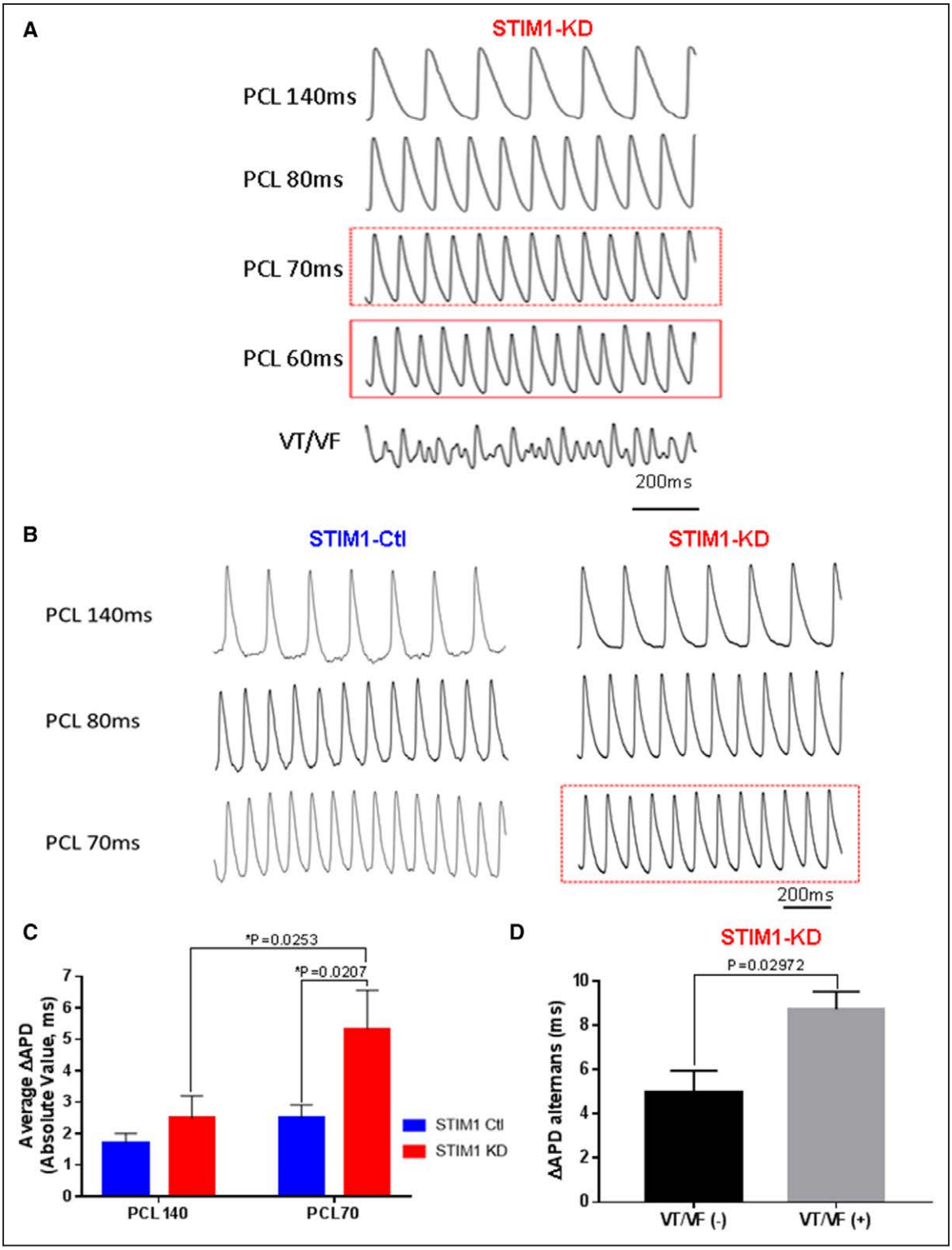

Figure 6. Pacing-induced action potential alternans in STIM1-KD (stromal interaction molecule 1 knockdown) hearts.
A, Representative action potential (AP) traces documenting the emergence of AP alternans before the onset of ventricular tachycardia/ventricular fibrillation (VT/VF) in STIM1-KD hearts. **B**, Representative AP traces during progressive elevation in pacing rate in STIM1-Ctl (control; left) and STIM1-KD (right) hearts illustrating presence of substantial pacing-induced AP alternans (red frame) in the latter but not former. **C**, Average ΔAPD_{75} measured at pacing cycle length 140 ms and 70 ms in STIM1-Ctl (n=7) andSTIM1-KD (n=6) hearts. Statistical analysis detailed in Table 2. **D**, Average ΔAPD_{75} as a measure of alternans magnitude in VT/VF(+) and VT/VF(–) STIM1-KD hearts. Statistical analysis: *t* test (*P*=0.0297). Data represent mean±SEM.

were prone to VT/VF exhibited markedly increased (by >60%, *P*<0.03) alternans magnitude relative to their VT/VF(–) counterparts (Figure 6D).

We then examined the spatio-temporal characteristics of APD alternans across the epicardial surface of STIM1-KD and STIM1-Ctl hearts (Figure 7A). Once

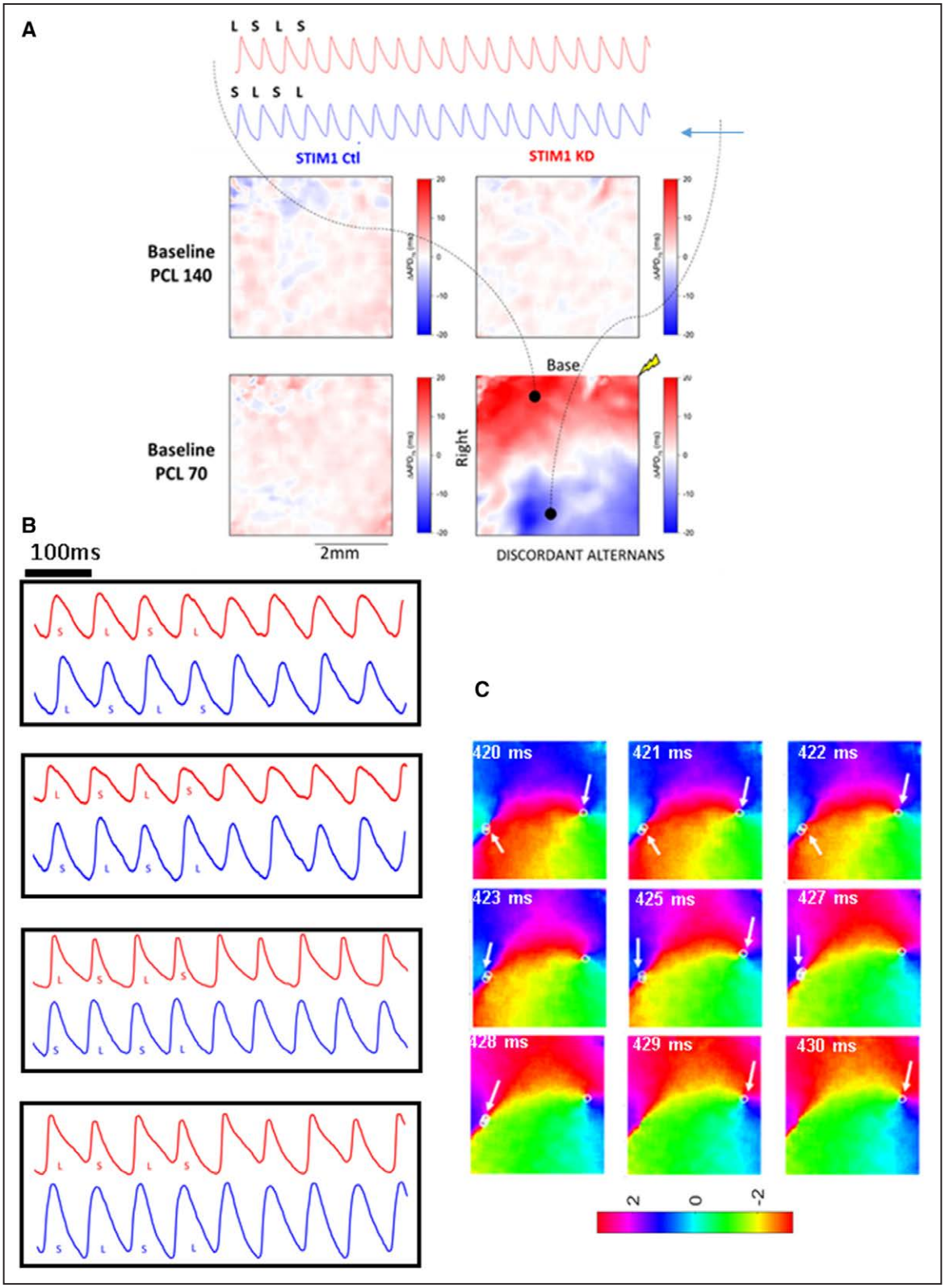

Figure 7. Spatially discordant action potential alternans and their relevance to functional reentry in STIM1-KD (stromal interaction molecule 1 knockdown) hearts.

A, Contour maps depicting the spatial distribution of ΔAPD_{75} in STIM1-Ctl (control; left) and STIM1-KD (right) hearts at basal pacing cycle length (PCL 140 ms) and elevated (PCL 70 ms) pacing rates. STIM1-KD but not STIM1-Ctl hearts exhibited a spatial discordant alternans profile marked by adjacent zones of opposite alternans polarity. Also shown are representative action potential tracings from the zones of opposite polarity illustrating the long (L)-short (S) (red) and short-long (blue) sequences. **B**, Examples of actions potential traces displaying discordant alternans in 4 different STIM1-KD hearts. **C**, Representative phase maps recorded during the early onset of ventricular tachycardia/ventricular fibrillation (VT/VF) showing stable rotors that are localized along the nodal line separating the out-of-phase alternans regions.

Table 2. Statistical Analysis of Average ΔAPD at PCL of 140 ms and 70 ms

2-Way ANOVA-Sidak's Multiple Comparisons Test	
STIM1-Ctl vs STIM-KD	
PCL 140	*P*=0.6918 (NS)
PCL 70	*P*=0.0207
PCL140 vs PCL70	
STIM1-Ctl	*P*=0.6617 (NS)
STIM1-KD	*P*=0.0253

ΔAPD is the difference in APD on 3 consecutive odd and even beats (APD alternans). APD indicates action potential duration; PCL, pacing cycle length; STIM1-Ctl, control mice without STIM1 depletion; and STIM1-KD, myocyte-restricted STIM1 knock-down.

again, a decrease in PCL from 140 ms to 70 ms did not result in a major change in the magnitude of APD alternans which remained minimal (<2–3 ms) in STIM1-Ctl hearts. In contrast, challenge of STIM1-KD hearts with an identical decrease in PCL led to the emergence of spatially discordant APD alternans in all arrhythmia-prone STIM1-KD hearts. Examples of discordant alternans from different hearts are presented in Figure 7B. The alternans profile of a representative STIM1-KD heart is shown in Figure 7A. Discrete zones of opposite ΔAPD_{75} polarity (long-short and short-long APD sequences) were formed (Figure 7A). These discrete zones of discordant alternans (red and blue regions) were separated by a nodal line of zero alternans (white border). The functional significance of the discordant alternans profile of STIM1-KD hearts is documented in Figure 7C. On further challenge with a more rapid pacing rate (PCL 50–60 ms), STIM1-KD hearts exhibiting spatially discordant alternans were prone to wavebreak formation and the generation of meandering spiral waves that gave rise to VT/VF. As predicted in theoretical studies,[28] our detailed phase mapping and phase singularity analysis during the early onset of VT/VF in STIM1-KD hearts localized the rotor cores along the nodal line separating the out-of-phase alternans regions (Figure 7C and Movie in the Data Supplement).

DISCUSSION

The main objective of the present study was to examine the in vivo role of cardiomyocyte STIM1 expression in the adult heart using an approach in which myocyte-specific STIM1 depletion is rapidly induced in adult mice. A major advantage of our experimental approach was the ability to avoid potentially confounding factors associated with long-term gene reprogramming in standard transgenic models, the extra-cardiac and nonmyocyte effects of STIM1 downregulation and upregulation in global gene manipulation models, and potentially artificial effects associated with excessive adenovirus-mediated STIM1 overexpression in adult myocytes in culture. Our study was motivated, in large part, by seemingly conflicting findings by us and others regarding the impact of altered STIM1 expression on myocardial properties of normal and stressed hearts. The major findings of the present report are as follows: (1) cardiomyocyte-restricted STIM1 depletion in the adult heart results in a severe phenotype marked by poor survival and a mortality rate >50% after only 8 days of gene knockdown, (2) STIM1-KD hearts exhibit hallmark features of pro-arrhythmic electrophysiological remodeling, including CV slowing and increased APD heterogeneity. (3) These changes are a direct consequence of cardiomyocyte STIM1 depletion as opposed to nonspecific LV dysfunction as they are neither observed in STIM-Ctl nor Cre-Ctl hearts which exhibited similar mechanical response to the tamoxifen regimen; (4) challenge of STIM1-KD but not STIM1-Ctl or Cre-Ctl hearts with rapid stimulus trains unmasks their marked susceptibility to sustained VT/VF, (5) VT/VF in this model is likely related to spatially discordant APD alternans that promote wavebreak formation and the development of rotor activity at the nodal line separating the out-of-phase regions.

Cardiomyocyte-Specific STIM1 KD in the adult Heart Causes Early Mortality

A completely unexpected outcome of our current study was the revelation that cardiomyocyte-specific STIM1 depletion causes rapid (within 5–6 days) onset of mortality that ultimately exceeds 50% after only 8 days of gene knockdown. This rise in mortality was related to STIM1 depletion per se, since survival of STIM1-Ctl and Cre-Ctl mice was not affected. While other tissue-specific STIM1 deletion models have also been associated with increased mortality, our STIM1-KD mice appear to exhibit a more severe phenotype.[7,12,21] For one, in a cardiomyocyte-restricted STIM1 knockout model ((cr)STIM1-KO) in which gene deletion is present throughout embryogenesis and early post-natal development, mice survived for at least 40 days before they underwent a rapid phase of mortality that was similar to what we report in our adult STIM1-KD mice.[7] This strongly suggests the possibility that STIM1 depletion does not adversely impact survival of neonatal hearts. Nonetheless, STIM1 expression is highly robust in the neonatal heart where it appears to play a critical role in SOCE-dependent signaling, a process which is not normally present in adult hearts.[9] Alternatively, gene expression reprogramming in response to embryonic STIM1 depletion may have improved survival of (cr)STIM1-KO mice through adaptive mechanisms which are avoided in our present study. Finally, the acute mortality rate that we report shortly after STIM1-KD in adult mice is reminiscent to that reported by Li et al[29] in neonatal mice with skeletal muscle STIM1 depletion.

STIM1-KD Hearts Are Prone to the Development of Arrhythmogenic Discordant Alternans

Another major finding of our study was the elucidation of the mechanism underlying the enhanced susceptibility of STIM1-KD mice to arrhythmias. While STIM1-KD hearts exhibited hallmark electrophysiological features of the failing heart, including substantial CV slowing and APD heterogeneity, these changes were not sufficient to explain the heightened pro-arrhythmic risk, as they were comparable in arrhythmia-prone and arrhythmia-free hearts. Instead, we found that rapid stimulation was very effective in unmasking the arrhythmic behavior of STIM1-KD mice by promoting a spatially discordant APD alternans profile. As predicted by computational modeling studies,[28] our experimental findings documented the localization of reentrant rotors along the nodal lines separating the out-of-phase alternans regions. The mechanism underlying the increased alternans magnitudes that we observed in STIM1-KD hearts is likely related to impaired SR Ca^{2+} reuptake at high stimulation frequencies. Indeed, previous studies have documented the link between impaired SR Ca^{2+} reuptake in heart failure and the increased magnitude of alternans,[30] as well as the utility of SERCA2a gene transfer in suppressing arrhythmogenic alternans.[31] In addition, CV slowing in STIM1-KD hearts may act to promote the magnitude of alternans by imposing long intraventricular delays that contribute to regional differences in the local diastolic interval, especially during rapid pacing. Of note, suppression of CV slowing by promoting gap junction coupling has been shown to suppress APD alternans.

Conclusions

The data presented here demonstrate that cardiomyocyte STIM1 depletion promotes the incidence of malignant ventricular arrhythmias that arise from spatially discordant action potential alternans. Our findings indicate that a basal level of STIM1 in the adult cardiomyocyte is required to maintain normal cardiac rhythm.

ARTICLE INFORMATION

Received March 12, 2019; accepted September 16, 2019.

The Data Supplement is available at https://www.ahajournals.org/doi/suppl/10.1161/CIRCEP.119.007382.

Correspondence

Fadi G. Akar, PhD, Cardiovascular Research Center, Icahn School of Medicine at Mt Sinai, New York 10029. Email fadi.akar@mssm.edu

Affiliations

Cardiovascular Research Center, Division of Cardiology, Icahn School of Medicine at Mount Sinai (M.C., B.S., N.R., Z.I., J.H., L.B., J.-S.H., F.G.A.). Department of Pathology, New York University School of Medicine (S.F.).

Sources of Funding

This work was supported by National Institutes of Health grants to Dr Akar (R01 HL091923, R01 HL136222 and R21AG054211) and Dr Feske (AI097302).

Disclosures

Dr Feske is a scientific cofounder of Calcimedica. The other authors report no conflicts.

REFERENCES

1. Collins HE, Zhu-Mauldin X, Marchase RB, Chatham JC. STIM1/Orai1-mediated SOCE: current perspectives and potential roles in cardiac function and pathology. *Am J Physiol Heart Circ Physiol*. 2013;305:H446–H458. doi: 10.1152/ajpheart.00104.2013
2. Kiviluoto S, Decuypere JP, De Smedt H, Missiaen L, Parys JB, Bultynck G. STIM1 as a key regulator for Ca2+ homeostasis in skeletal-muscle development and function. *Skelet Muscle*. 2011;1:16. doi: 10.1186/2044-5040-1-16
3. Stiber J, Hawkins A, Zhang ZS, Wang S, Burch J, Graham V, Ward CC, Seth M, Finch E, Malouf N, Williams RS, Eu JP, Rosenberg P. STIM1 signalling controls store-operated calcium entry required for development and contractile function in skeletal muscle. *Nat Cell Biol*. 2008;10:688–697. doi: 10.1038/ncb1731
4. Kassan M, Ait-Aissa K, Radwan E, Mali V, Haddox S, Gabani M, Zhang W, Belmadani S, Irani K, Trebak M, Matrougui K. Essential role of smooth muscle STIM1 in hypertension and cardiovascular dysfunction. *Arterioscler Thromb Vasc Biol*. 2016;36:1900–1909. doi: 10.1161/ATVBAHA.116.307869
5. Ross GR, Bajwa T Jr, Edwards S, Emelyanova L, Rizvi F, Holmuhamedov EL, Werner P, Downey FX, Tajik AJ, Jahangir A. Enhanced store-operated Ca2+ influx and ORAI1 expression in ventricular fibroblasts from human failing heart. *Biol Open*. 2017;6:326–332. doi: 10.1242/bio.022632
6. Zhang B, Jiang J, Yue Z, Liu S, Ma Y, Yu N, Gao Y, Sun S, Chen S, Liu P. Store-Operated Ca2+ Entry (SOCE) contributes to angiotensin II-induced cardiac fibrosis in cardiac fibroblasts. *J Pharmacol Sci*. 2016;132:171–180. doi: 10.1016/j.jphs.2016.05.008
7. Collins HE, He L, Zou L, Qu J, Zhou L, Litovsky SH, Yang Q, Young ME, Marchase RB, Chatham JC. Stromal interaction molecule 1 is essential for normal cardiac homeostasis through modulation of ER and mitochondrial function. *Am J Physiol Heart Circ Physiol*. 2014;306:H1231–H1239. doi: 10.1152/ajpheart.00075.2014
8. Nakipova OV, Averin AS, Evdokimovskii EV, Pimenov OY, Kosarski L, Ignat'ev D, Anufriev A, Kokoz YM, Reyes S, Terzic A, Alekseev AE. Store-operated Ca2+ entry supports contractile function in hearts of hibernators. *PLoS One*. 2017;12:e0177469. doi: 10.1371/journal.pone.0177469
9. Luo X, Hojayev B, Jiang N, Wang ZV, Tandan S, Rakalin A, Rothermel BA, Gillette TG, Hill JA. STIM1-dependent store-operated Ca^{2+} entry is required for pathological cardiac hypertrophy. *J Mol Cell Cardiol*. 2012;52:136–147. doi: 10.1016/j.yjmcc.2011.11.003
10. Hulot JS, Fauconnier J, Ramanujam D, Chaanine A, Aubart F, Sassi Y, Merkle S, Cazorla O, Ouillé A, Dupuis M, Hadri L, Jeong D, Mühlstedt S, Schmitt J, Braun A, Bénard L, Saliba Y, Laggerbauer B, Nieswandt B, Lacampagne A, Hajjar RJ, Lompré AM, Engelhardt S. Critical role for stromal interaction molecule 1 in cardiac hypertrophy. *Circulation*. 2011;124:796–805. doi: 10.1161/CIRCULATIONAHA.111.031229
11. Ohba T, Watanabe H, Murakami M, Sato T, Ono K, Ito H. Essential role of STIM1 in the development of cardiomyocyte hypertrophy. *Biochem Biophys Res Commun*. 2009;389:172–176. doi: 10.1016/j.bbrc.2009.08.117
12. Correll RN, Goonasekera SA, van Berlo JH, Burr AR, Accornero F, Zhang H, Makarewich CA, York AJ, Sargent MA, Chen X, Houser SR, Molkentin JD. STIM1 elevation in the heart results in aberrant Ca^{2+} handling and cardiomyopathy. *J Mol Cell Cardiol*. 2015;87:38–47. doi: 10.1016/j.yjmcc.2015.07.032
13. Ohba T, Watanabe H, Murakami M, Iino K, Adachi T, Baba Y, Kurosaki T, Ono K, Ito H. Stromal interaction molecule 1 haploinsufficiency causes maladaptive response to pressure overload. *PLoS One*. 2017;12:e0187950. doi: 10.1371/journal.pone.0187950
14. Parks C, Alam MA, Sullivan R, Mancarella S. STIM1-dependent Ca(2+) microdomains are required for myofilament remodeling and signaling in the heart. *Sci Rep*. 2016;6:25372. doi: 10.1038/srep25372
15. Bénard L, Oh JG, Cacheux M, Lee A, Nonnenmacher M, Matasic DS, Kohlbrenner E, Kho C, Pavoine C, Hajjar RJ, Hulot JS. Cardiac stim1 silencing impairs adaptive hypertrophy and promotes heart failure through

inactivation of mTORC2/Akt signaling. *Circulation*. 2016;133:1458–71; discussion 1471. doi: 10.1161/CIRCULATIONAHA.115.020678
16. Zhao G, Li T, Brochet DX, Rosenberg PB, Lederer WJ. STIM1 enhances SR Ca2+ content through binding phospholamban in rat ventricular myocytes. *Proc Natl Acad Sci U S A*. 2015;112:E4792–E4801. doi: 10.1073/pnas.1423295112
17. Avila-Medina J, Mayoral-Gonzalez I, Dominguez-Rodriguez A, Gallardo-Castillo I, Ribas J, Ordoñez A, Rosado JA, Smani T. The complex role of store operated calcium entry pathways and related proteins in the function of cardiac, skeletal and vascular smooth muscle cells. *Front Physiol*. 2018;9:257. doi: 10.3389/fphys.2018.00257
18. Bootman MD, Rietdorf K. Tissue specificity: store-operated Ca2+ entry in cardiac myocytes. *Adv Exp Med Biol*. 2017;993:363–387. doi: 10.1007/978-3-319-57732-6_19
19. Liu J, Xin L, Benson VL, Allen DG, Ju YK. Store-operated calcium entry and the localization of STIM1 and Orai1 proteins in isolated mouse sinoatrial node cells. *Front Physiol*. 2015;6:69. doi: 10.3389/fphys.2015.00069
20. Liu R, Correll RN, Davis J, Vagnozzi RJ, York AJ, Sargent MA, Nairn AC, Molkentin JD. Cardiac-specific deletion of protein phosphatase 1β promotes increased myofilament protein phosphorylation and contractile alterations. *J Mol Cell Cardiol*. 2015;87:204–213. doi: 10.1016/j.yjmcc.2015.08.018
21. Zhang H, Sun AY, Kim JJ, Graham V, Finch EA, Nepliouev I, Zhao G, Li T, Lederer WJ, Stiber JA, Pitt GS, Bursac N, Rosenberg PB. STIM1-Ca2+ signaling modulates automaticity of the mouse sinoatrial node. *Proc Natl Acad Sci U S A*. 2015;112:E5618–E5627. doi: 10.1073/pnas.1503847112
22. Oh-Hora M, Yamashita M, Hogan PG, Sharma S, Lamperti E, Chung W, Prakriya M, Feske S, Rao A. Dual functions for the endoplasmic reticulum calcium sensors STIM1 and STIM2 in T cell activation and tolerance. *Nat Immunol*. 2008;9:432–443. doi: 10.1038/ni1574
23. Xie C, Hu J, Motloch LJ, Karam BS, Akar FG. The classically cardioprotective agent diazoxide elicits arrhythmias in type 2 diabetes mellitus. *J Am Coll Cardiol*. 2015;66:1144–1156. doi: 10.1016/j.jacc.2015.06.1329
24. Akar FG, Aon MA, Tomaselli GF, O'Rourke B. The mitochondrial origin of postischemic arrhythmias. *J Clin Invest*. 2005;115:3527–3535. doi: 10.1172/JCI25371
25. Akar FG, Yan GX, Antzelevitch C, Rosenbaum DS. Unique topographical distribution of M cells underlies reentrant mechanism of torsade de pointes in the long-QT syndrome. *Circulation*. 2002;105:1247–1253. doi: 10.1161/hc1002.105231
26. Bray MA, Wikswo JP. Considerations in phase plane analysis for nonstationary reentrant cardiac behavior. *Phys Rev E Stat Nonlin Soft Matter Phys*. 2002;65(5 Pt 1):051902. doi: 10.1103/PhysRevE.65.051902
27. Umapathy K, Nair K, Masse S, Krishnan S, Rogers J, Nash MP, Nanthakumar K. Phase mapping of cardiac fibrillation. *Circ Arrhythm Electrophysiol*. 2010;3:105–114. doi: 10.1161/CIRCEP.110.853804
28. Gaeta SA, Christini DJ. Non-linear dynamics of cardiac alternans: subcellular to tissue-level mechanisms of arrhythmia. *Front Physiol*. 2012;3:157. doi: 10.3389/fphys.2012.00157
29. Li T, Finch EA, Graham V, Zhang ZS, Ding JD, Burch J, Oh-hora M, Rosenberg P. STIM1-Ca(2+) signaling is required for the hypertrophic growth of skeletal muscle in mice. *Mol Cell Biol*. 2012;32:3009–3017. doi: 10.1128/MCB.06599-11
30. Wilson LD, Jeyaraj D, Wan X, Hoeker GS, Said TH, Gittinger M, Laurita KR, Rosenbaum DS. Heart failure enhances susceptibility to arrhythmogenic cardiac alternans. *Heart Rhythm*. 2009;6:251–259. doi: 10.1016/j.hrthm.2008.11.008
31. Cutler MJ, Wan X, Plummer BN, Liu H, Deschenes I, Laurita KR, Hajjar RJ, Rosenbaum DS. Targeted sarcoplasmic reticulum Ca2+ ATPase 2a gene delivery to restore electrical stability in the failing heart. *Circulation*. 2012;126:2095–2104. doi: 10.1161/CIRCULATIONAHA.111.071480